Monthly Notices of the ROYAL ASTRONOMICAL SOCIETY

MNRAS **467,** 3712–3722 (2017)
Advance Access publication 2017 January 7

doi:10.1093/mnras/stx022

Evidence of bar-driven secular evolution in the gamma-ray narrow-line Seyfert 1 galaxy FBQS J164442.5+261913

A. Olguín-Iglesias,[1,2★] J. K. Kotilainen,[2★] J. León Tavares,[3] V. Chavushyan[1] and C. Añorve[4]

[1]*Instituto Nacional de Astrofísica Óptica y Electrónica (INAOE), Apartado Postal 51 y 216, 72000 Puebla, México*
[2]*Finnish Centre for Astronomy with ESO (FINCA), University of Turku, Väisäläntie 20, FI-21500 Piikkiö, Finland*
[3]*Sterrenkundig Observatorium, Universiteit Gent, Krijgslaan 281-S9, B-9000 Gent, Belgium*
[4]*Facultad de Ciencias de la Tierra y del Espacio, de la Universidad Autónoma de Sinaloa, Blvd. de las Américas y Av. Universitarios S/N, Ciudad Universitaria, C.P. 80010, Culiacán Sinaloa, México*

Accepted 2017 January 4. Received 2017 January 4; in original form 2016 November 1

ABSTRACT

We present near-infrared imaging of FBQS J164442.5+261913, one of the few γ-ray emitting narrowline Seyfert 1 galaxies detected at high significance level by *Fermi* Large Area Telescope. This study is the first morphological analysis performed of this source and the third performed of this class of objects. Conducting a detailed 2D modelling of its surface brightness distribution and analysing its $J - K_s$ colour gradients, we find that FBQS J164442.5+261913 is statistically most likely hosted by a barred lenticular galaxy (SB0). We find evidence that the bulge in the host galaxy of FBQS J164442.5+261913 is not classical but pseudo, against the paradigm of powerful relativistic jets exclusively launched by giant ellipticals. Our analysis also reveals the presence of a ring with diameter equalling the bar length ($r_{\rm bar} = 8.13 \pm 0.25$ kpc), whose origin might be a combination of bar-driven gas rearrangement and minor mergers, as revealed by the apparent merger remnant in the *J*-band image. In general, our results suggest that the prominent bar in the host galaxy of FBQS J164442.5+261913 has mostly contributed to its overall morphology driving a strong secular evolution, which plays a crucial role in the onset of the nuclear activity and the growth of the massive bulge. Minor mergers, in conjunction, are likely to provide the necessary fresh supply of gas to the central regions of the host galaxy.

Key words: galaxies: active – galaxies: evolution – galaxies: interactions – galaxies: jets – galaxies: photometry – galaxies: Seyfert.

1 INTRODUCTION

Narrow-line Seyfert 1 (NLSy1) galaxies are type 1 active galactic nuclei (AGN) characterized by narrower Balmer lines [FWHM(Hβ) $< 2000\,{\rm km\,s^{-1}}$] than in normal Seyferts, flux ratios [O III]/Hβ < 3, strong optical Fe II lines (Fe II bump) and a soft X-ray excess (Osterbrock & Pogge 1985; Pogge 2000). Based on the full width at half-maximum (FWHM) of their broad-line region (BLR) lines and the continuum luminosity (Kaspi et al. 2000), their central black holes masses ($M_{\rm BH}$) are estimated to range from $\sim 10^6$ to $\sim 10^7\,{\rm M}_\odot$ (Mathur et al. 2012, although Baldi et al. 2016 show that these low $M_{\rm BH}$ estimates might be seriously affected by the orientation of the BLR). Their low-mass black holes suggest that their accretion rates are close to the Eddington limit and their host galaxies are in an early phase of galaxy evolution (Ohta et al. 2007). Unfortunately, relatively little is known about their host galaxies.

Some studies find that their morphologies resemble those of inactive spirals with a regular presence of stellar bars (Crenshaw, Kraemer & Gabel 2003) and pseudo-bulges (Orban de Xivry et al. 2011; Mathur et al. 2012). However, γ-ray emission have been detected in seven radio-loud NLSy1 (RL-NLSy1) by the Large Area Telescope (LAT) on board the *Fermi* satellite, suggesting that highly beamed and strongly collimated relativistic jets can be launched by RL-NLSy1 AGN. The latter, challenge the paradigm that such jets are launched exclusively by blazars hosted by giant elliptical galaxies (Laor 2000; Marscher 2009) with black holes with masses $M_{\rm BH} \gtrsim 10^8\,{\rm M}_\odot$ accreting at low rates (McLure et al. 2004; Sikora, Stawarz & Lasota 2007). Therefore, a thorough analysis of the host galaxies of this new class of AGN (hereafter γ-NLSy1; Abdo et al. 2009), becomes a priority.

So far, only two γ-NLSy1 host galaxies have been characterized, 1H 0323+342 (Antón, Browne & Marchã 2008;

★ E-mail: alejandroolguiniglesias@gmail.com (AO-I); jarkot@utu.fi (JKK)

León Tavares et al. 2014) and PKS 2004−447 (Kotilainen et al. 2016). These studies reveal characteristics such as the presence of discs, rings, bars and pseudo-bulges, which are expected in normal NLSy1s, however, do not fit with the common belief that powerful relativistic jets are launched exclusively by giant ellipticals.

As part of our ongoing imaging survey of the complete sample of γ-NLSy1 galaxies detected so far, we conducted near-infrared (NIR, J and K_s bands) observations to the γ-NLSy1 FBQS J164442.5+261913. This is one of the sources detected by *Fermi* LAT with high significance, having test statistic TS $>$ 25 ($\sim 5\sigma$; Mattox et al. 1996) and given its redshift ($z = 0.145$; Bade et al. 1995), it is the second closest after 1H 0323+342 ($z = 0.061$), making it an excellent candidate for accurate morphological studies to its host galaxy. With the aim of achieving a better understanding of the mechanisms needed to form and develop highly collimated relativistic jets, in this paper we present the results from our thorough analysis to FBQS J164442.5+261913.

This paper is structured as follows: observations and data reduction are presented in Section 2; the methods we adopt to analyse the data are explained in Section 3. Our results and discussion are presented in Sections 4 and 5. In Section 6, we summarize our findings. Throughout the manuscript, we adopt a concordance cosmology with $\Omega_{\rm m} = 0.3$, $\Omega_\Lambda = 0.7$ and a Hubble constant of $H_0 = 70$ Mpc^{-1} km s^{-1}.

2 OBSERVATIONS AND DATA REDUCTION

The J- and K-band observations of FBQS J164442.5+261913 were conducted at the 2.5 m Nordic Optical Telescope (NOT) during the night of 2015 May 1 using the wide-field NIR camera NOTcam with CCD dimensions of 1024 pixels × 1024 pixels and a pixel scale of 0.234 arcsec pix^{-1}, giving a field of view (FOV) of $\sim 4 \times 4$ arcmin^2. During the night, the seeing was very good, with an average FWHM of $\sim$0.75 and $\sim$0.63 arcsec for J and K_s bands, respectively. The target was imaged using the NOTcam standard J ($\lambda_{\rm central} = 1.246$ μm) and K_s ($\lambda_{\rm central} = 2.140$ μm) filters with a dithering technique with individual exposures of 30 s and a typical offset of $\sim$10 arcsec. A total of 85 individual exposures for J band and 72 for K_s band were obtained, giving a total exposure time of 2550 and 2160 s, respectively.

The data reduction was performed using the NOTcam reduction package[1] for IRAF[2]. First we corrected for the optical distortion of the wide-field camera using distortion models based on high-quality data of a stellar-rich field. Then, bad pixels were masked out using a file available in the NOTCam, bad pixel mask archive. A normalized flat-field was created from evening and morning sky frames to account for the thermal contribution. Using field stars as reference points, the dittered images were aligned and co-added to obtain the final reduced image used in our analysis. In order to perform photometric calibration to the images, we retrieved J- and K_s-band magnitudes from 2MASS (Skrutskie et al. 2006) resulting in an accuracy of $\sim$0.10 mag. The derived integrated magnitudes in circular apertures are $m_J = 15.35 \pm 0.10$ ($M_J = -23.84 \pm 0.10$) and $m_{Ks} = 13.44 \pm 0.10$ ($M_{Ks} = -25.86 \pm 0.10$). Galactic extinction for J and K_s bands are negligible ($A_\lambda[J] = 0.058$ and $A_\lambda[K_s] = 0.025$).

[1] www.not.iac.es/instruments/notcam/.

[2] IRAF is distributed by the National Optical Astronomy Observatories, which are operated by the Association of Universities for Research in Astronomy, Inc., under cooperative agreement with the National Science Foundation.

3 IMAGE ANALYSIS

3.1 Photometric decomposition

We perform a 2D modelling of the galaxy using the image decomposition code GALFIT (Peng et al. 2011). We follow the procedure described in our previous studies of AGN host galaxies (León Tavares et al. 2014; Olguín-Iglesias et al. 2016), which is described below.

The first and most important part of the analysis is the modelling of the point spread function (PSF) by fitting selected stars of the FOV (Fig. 1). These stars are non-saturated, with no sources within $\sim$7 arcsec radius, more than $\sim$10 arcsec away from the border of the FOV and with a range of magnitudes that allow us a proper characterization of core and wings. Stars 2, 5, 6, 8 and 9 fulfil these criteria (see Fig. 1) and thus are used to derive our PSF model. On the other hand, star 1 is saturated, stars 3 and 10 are very close to the border of the FOV and stars 4 and 7 have close companions.

Each selected star is centred in a 50 × 50 arcsec^2 box, where all extra sources are masked out by implementing the segmentation image process of SEXTRACTOR (Bertin & Arnouts 1996). The stars are simultaneously modelled, using one Gaussian function (intended to fit the core of the stars) then, the resulting model is added with an exponential function (intended to fit the wings of the stars). Similarly, depending on the residuals, we add extra Gaussians and exponential functions until the core and wings are satisfactorily fitted. For our imagery, six Gaussians and six exponentials (and a flat plane that fits the sky background) were enough. The result is considered as a suitable PSF model for our analysis once it successfully fits all the stars individually (Fig. 2).

Next, we fit FBQS J164442.5+261913 with the scaled version of our derived PSF as the only component, to constrain the unresolved AGN contribution at the centre of the galaxy. Since the residuals of the single PSF model (hereafter model 1) are considerable ($\chi^2_{\rm model1} = 4.148 \pm 0.01$ for J band and $\chi^2_{\rm model1} = 3.171 \pm 0.02$ for K_s band), we continue our analysis by adding extra functions to the model. We use the Sérsic profile, expressed such that

$$I(R) = I_e \exp\left[-\kappa_n\left(\left(\frac{R}{R_e}\right)^{1/n} - 1\right)\right], \quad (1)$$

where $I(R)$ is the surface brightness at the radius R, and κ_n is a parameter coupled to the Sérsic index n in such a way that I_e is the surface brightness at the effective radius R_e, where the galaxy contains half of the light (Graham & Driver 2005). The Sérsic profile has the ability to represent different stellar distributions such as elliptical galaxies, classical and pseudo-bulges and bars, just by varying its Sérsic index n. Hence, when $n = 4$, the Sérsic function is known as the de Vaucouleurs profile (widely used to fit elliptical galaxies and classical bulges); when $n = 1$, it is an exponential function, and when $n = 0.5$, it is a Gaussian.

Given that NLSy1s are known to be typically hosted in disc galaxies (Crenshaw, Kraemer & Gabel 2003), we also explore models that include the exponential function, expressed as

$$I(R) = I_0 \exp\left(\frac{R}{h_r}\right), \quad (2)$$

where $I(R)$ is the surface brightness at the radius R, I_0 is the central surface brightness and h_r is the disc scalelength.

3.1.1 Uncertainties

Since the error bars produced by GALFIT are purely statistical and thus, unrealistically small (Häussler et al. 2007; Bruce et al. 2012), we follow Kotilainen et al. (2011) and León Tavares et al. (2014) to

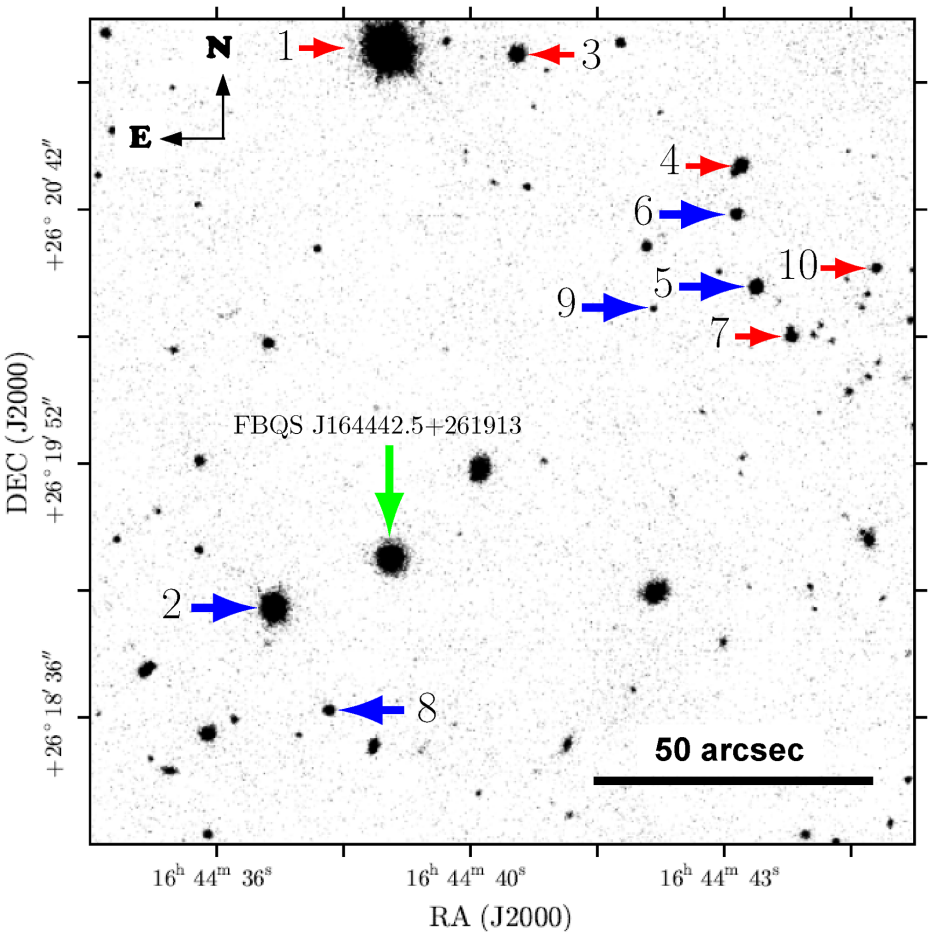

Figure 1. *J*-band NOTcam image of FBQS J164442.5+261913. The large green vertical arrow indicates the location of the target. Horizontal arrows show the suitable (blue thick arrows) and unsuitable (red thin arrows) stars for the PSF construction.

derive the uncertainties of our fittings. We identify model parameters that could contribute most significantly to errors. Regarding the PSF, spatial variations might affect the structural parameters of the galaxy model and, to a lesser extent, its magnitudes. To account for this, we compare the brightness distribution of our PSF model with the brightness distribution of each star in the field, whose only difference is assumed to lie in their positions.

On the other hand, sky background can affect magnitudes in a larger extent (when compared to the PSF) and to a lesser extent (yet significantly), the structural parameters of the galaxy model. Even though, our imagery is in NIR bands and thus the sky counts are SKYCOUNTS ≈ 0, they may show large variations. To account for this, we run several sky fits in separated regions of 300×300 pixels^2 (70×70 arcsec^2) and use the mean and $\pm 1\sigma$ of the resultant values to fit the galaxy. The outcomes are models with slightly different magnitudes that are assumed to be the errors due to the sky background.

Model magnitudes are also affected by uncertainties in the zero-point, estimated from magnitudes retrieved from 2MASS. Thus, zero-point magnitude variations (± 0.1mag) are also added as errors in the magnitudes of our final models.

3.2 Fit of the isophotes

Additionally to the morphological decomposition, we perform an analysis based on the ellipse fit to the galaxy isophotes (Wozniak et al. 1995; Knapen, Shlosman & Peletier 2000; Laine et al. 2002; Sheth et al. 2003; Elmegreen, Elmegreen & Hirst 2004; Marinova & Jogee 2007; Barazza, Jogee & Marinova 2008). We perform this analysis using the ELLIPSE task in IRAF. This procedure reads a 2D image to fit isophotes to its light distribution. The fits start from an initial guess of x and y centre, ellipticity (ϵ) and position angle (PA). Each extracted isophote is represented by its surface brightness (μ), semimajor axis length (R), PA and ϵ.

The fitted isophotes are used to represent and analyse the azimuthally averaged surface brightness profiles of the galaxy and the models derived from the photometric decomposition. Furthermore, the sample of isophotes extracted are used to identify changes in PA and ellipticity that could be associated with different structures within the galaxy morphology.

4 STRUCTURE OF FBQS J164442.5+261913

In order to characterize the morphology of FBQS J164442.5+261913, we first assume that it is hosted by an elliptical galaxy, since only these type of galaxies are known to launch powerful relativistic jets able to produce γ-rays (Marscher 2009). Thus, we add a Sérsic profile to the single PSF model that represents the AGN contribution. We constrain the Sérsic index to $n > 2.0$, given the observational evidence that the light profiles of most ellipticals and classical bulges, are better

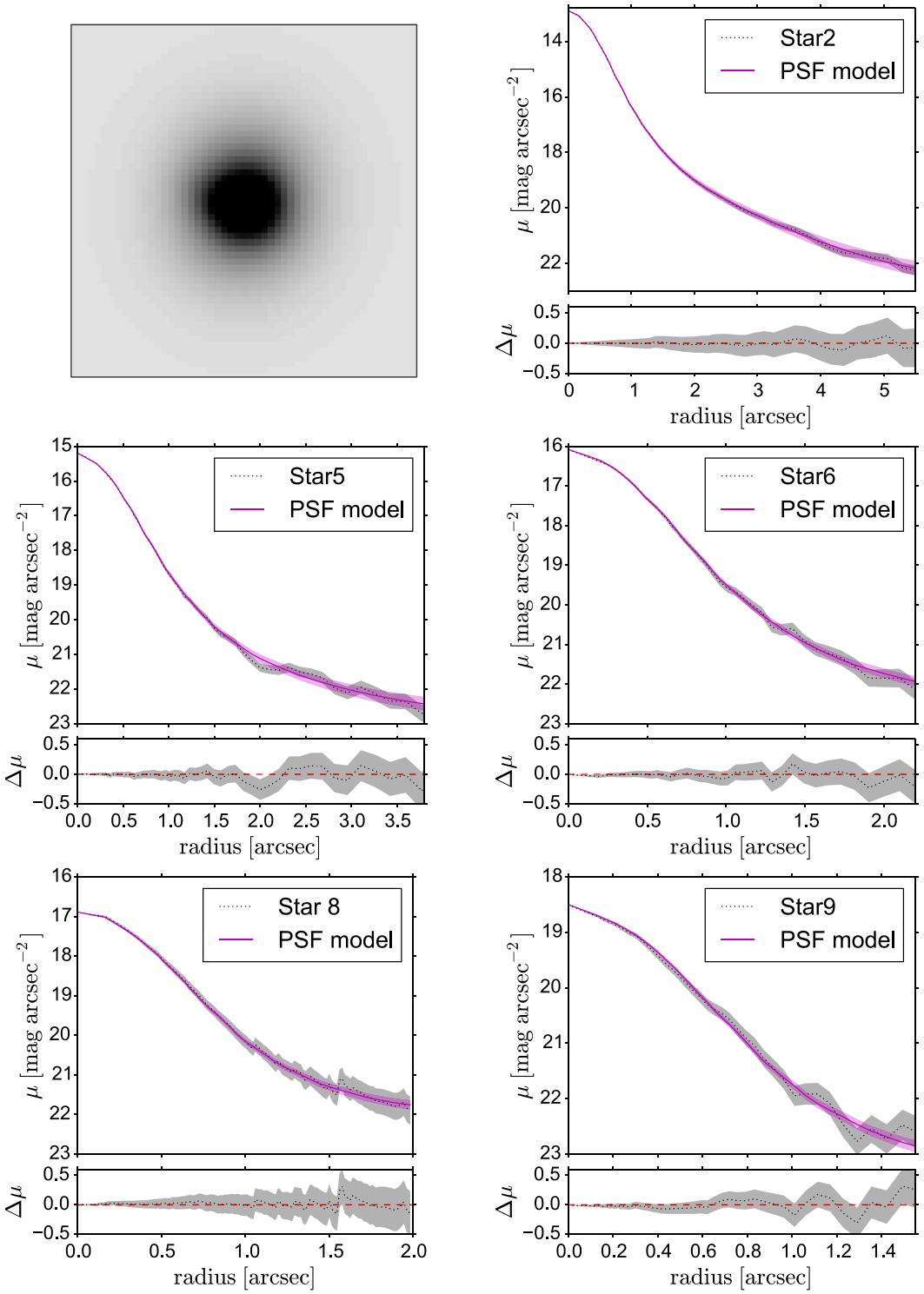

Figure 2. Test of the PSF model (top left image). Each star is fitted with our final PSF model in order to ensure its reliability. The top subpanel of each plot shows the azimuthally averaged surface brightness profiles of the PSF model (magenta line) and the fitted star (black data points). The lower subpanel shows the residuals of the fit.

described by a Sérsic function with $n > 2$, whereas most disc-like bulges have $n < 2$ (Fisher & Drory 2008; Gadotti 2009).

By means of a χ^2 test, we find that the improvement of this model (hereafter model 2) is equal for the J and the Ks bands ($\chi^2_{\rm model2}/\chi^2_{\rm model1} = 0.42$ for J band and $\chi^2_{\rm model2}/\chi^2_{\rm model1} = 0.42$ for K_s band). The images of the galaxy and the models, as well as the azimuthally average surface brightness profiles of the galaxy, the model and the sub-components of the model for each band are shown in Fig. 3.

The residual image of the J band from model 2 (top panel of Fig. 4), shows a ring-like feature interrupted in the eastern part. Neither the residuals nor the surface brightness profiles of the stars

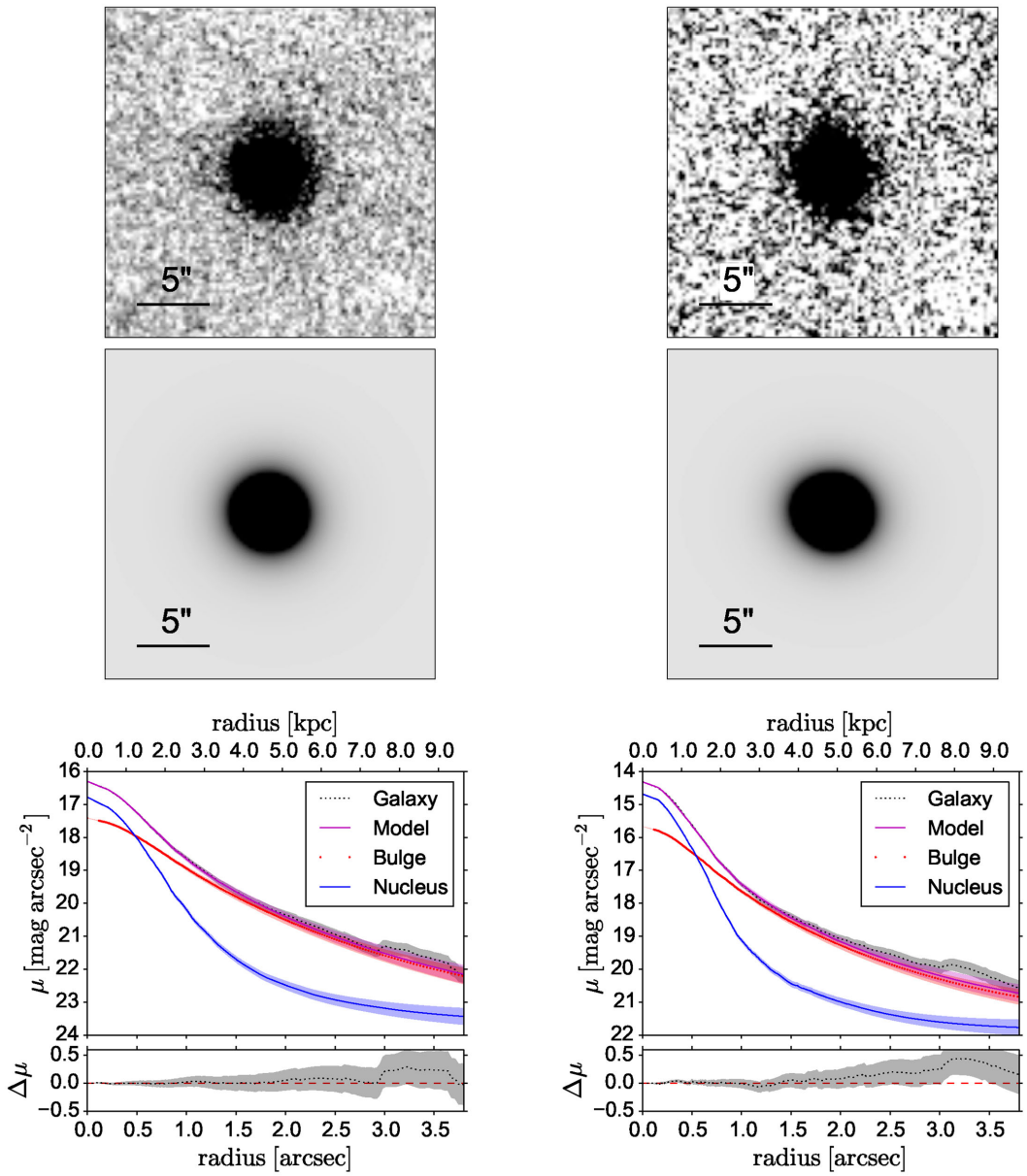

Figure 3. Model 2 (AGN+bulge). North is up and east is to the left. Left-hand column shows the *J* band and right-hand column shows the K_s band. Top row shows the observed images. Middle row shows the models images. Lower row shows the azimuthally averaged surface brightness profiles of the target, the model and the subcomponents of the model (top panel) and its residuals (bottom panel). Symbols are explained in the plots.

fitted with our PSF model show similar features. Moreover, its radius (∼3.5 arcsec) exceeds by far the FWHM of our PSF (∼0.75 arcsec). Hence, we consider the ring as a real component of the host galaxy.

The K_s-band residual (top panel of Fig. 5) shows an elongated and roughly symmetric structure with a length similar to the diameter of the ringed feature (∼3.2 arcsec/∼8.1 kpc). In both bands, a not-fitted bump in the light distribution of the galaxy is observed (from ∼2.8 to ∼3.7 arcsec), which is consistent with the ring and the two light enhancements close to the ends of the elongated structure. Since residuals are still considerable, we include an extra component into the last model (Fig. 6). We choose an exponential function, since it is able to represent the likely presence of a disc in the host galaxy of a typical NLSy1 galaxy (we call it model 3). The improvement over model 2 is $\chi^2_{\rm model3}/\chi^2_{\rm model2} = 0.65$ for *J* band and $\chi^2_{\rm model3}/\chi^2_{\rm model2} = 0.79$ for K_s band. From the residual images, we observe that the ring in *J* band (bottom panel of Fig. 4) seems better defined. Moreover, in K_s band (middle panel of Fig. 5), hints of this structure emerge, whereas the elongated structure disappearss.

The elongated feature and the light enhancements might be explained by the presence of a stellar bar showing their ansae (bright regions at the ends of bars observed in ∼40 per cent of SB0 galaxies, as found by Laurikainen et al. 2007; Martinez-Valpuesta, Knapen & Buta 2007). Such a bar could be more likely detected in K_s band since neither young luminous stars or dust strongly affect its observed emission (Rix & Rieke 1993). Nevertheless, a powerful AGN, a bright bulge and a disc, might outshine the bar, making its presence less evident. The upper panels of Fig. 7 show an image of FBQS J164442.5+261913 in K_s band, with the AGN and bulge contribution subtracted (using a bulge + AGN + disc model), revealing

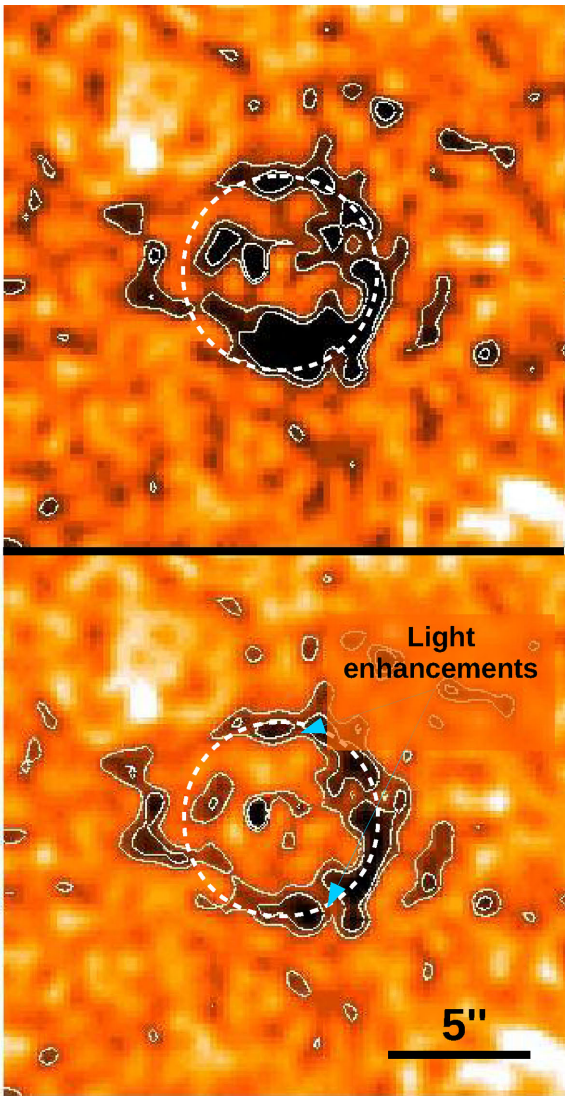

Figure 4. Residuals of the *J*-band model 2 (AGN+bulge, top panel) and model 3 (AGN+bulge+disc, bottom panel). North is up and east is to the left. To enhance S/N and to detect faint structures, the residuals were smoothed to <1 arcsec resolution. The segmented white circle has a 3.2 arcsec radius and guides through the ring feature. Blue arrows show the light enhancements at the ends of the bar (ansae). A likely minor merger event feature is observed in the east part of the galaxy (from $R \approx 3$ up to 5 arcsec), with a surface brightness in *J* band $\mu = 21.0 \pm 0.5$ mag arcsec^{-2}, which originates the blue region at 3 arcsec in the $J - K_s$ colour profile of Fig. 9.

an elongated and symmetrical feature that resembles a stellar bar over the underlying disc.

In order to confirm the existence of a bar in the host galaxy of FBQS J164442.5+261913, we perform another widely used method for detecting and describing bars; the ellipse fit of the galaxy isophotes (see plot in the lower panel of Fig. 7). When ϵ and PA are plotted against radius, a bar is characterized by a local maximum in ϵ and a constant PA (typically ΔPA $\lesssim 20^{\circ}$) along the bar (Wozniak et al. 1995; Jogee, Kenney & Smith 1999; Menéndez-Delmestre et al. 2007). We can see a region that fulfils these criteria (from $\sim$2.6 arcsec < radius < $\sim$3.2arcsec and PA $\sim 78^{\circ}$) suggesting again the presence of a bar. Since the method of the ellipses fit also hints at the presence of a bar, we proceed to characterize its morphology (Fig. 8). We add a Sérsic profile to model 3 of

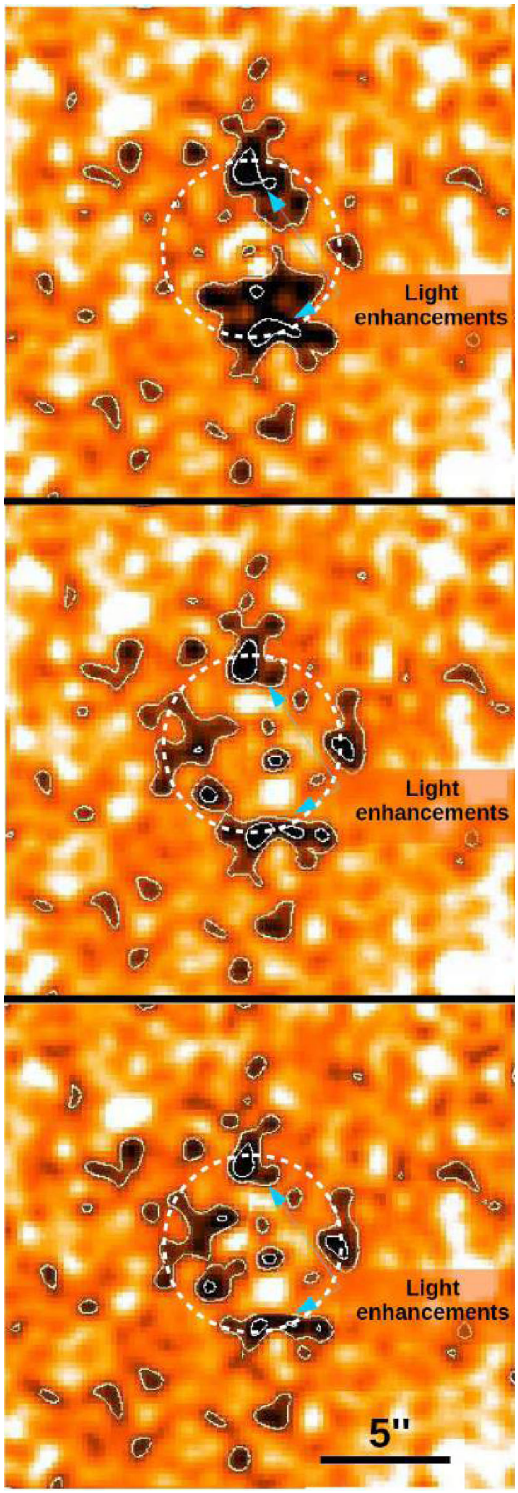

Figure 5. Residuals for the K_s-band model 2 (AGN+bulge, top panel), model 3 (AGN+bulge+disc, middle panel) and model 4 (AGN+bulge+disc+bar, bottom panel). North is up and east is to the left. To enhance S/N and to detect faint structures, the residuals were smoothed to <1 arcsec resolution. The segmented white circle has a 3.2 arcsec radius and guides through the ring feature. Blue arrows show the light enhancements at the ends of the bar (ansae). The residuals of model 2 shows hints of the bar, whereas the residuals of the models where we include a disc and a bar (models 3 and 4), show hints of the ring and the likely minor merger (eastern part of the galaxy, inside the white circle,) shown in *J* band.

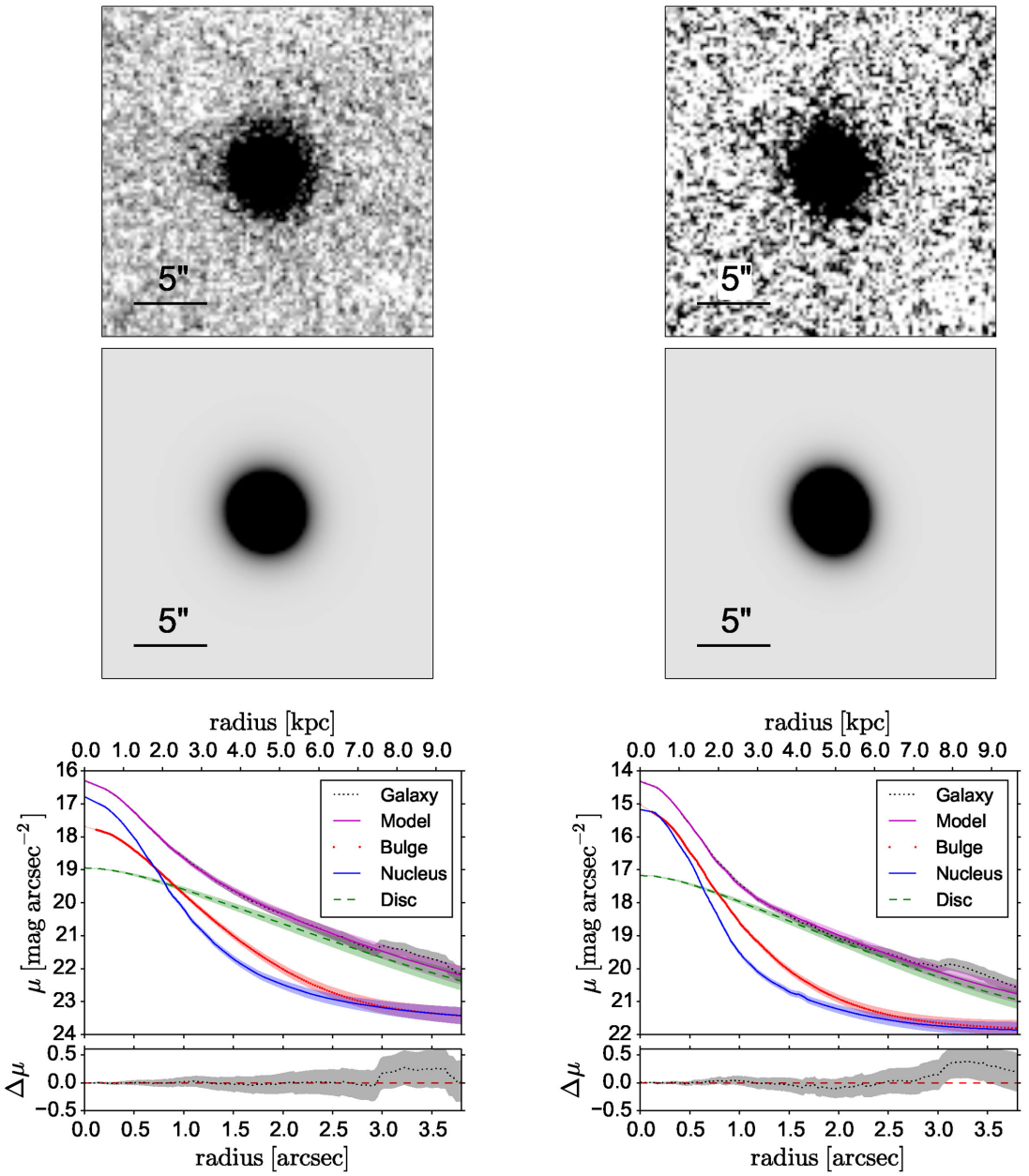

Figure 6. Model 3 (AGN+bulge+disc) for FBQS J164442.5+261913. Left-hand column shows the *J* band and right-hand column shows the K_s band. Top row shows the observed images. Middle row shows the images of our models. Lower row shows the azimuthally averaged surface brightness profiles of the target, the model and the subcomponents of the model (top panel) and its residuals (bottom panel). Symbols are explained in the plots.

K_s band to fit the light distribution of the stellar bar (we call it model 4). We use as initial guesses a Sérsic index $n = 0.5$ (Greene, Ho & Barth 2008) and the ϵ and PA derived from the ellipse fit of Fig. 7. The improvement with respect to the model where no bar is included is $\chi^2_{\rm model4}/\chi^2_{\rm model3} = 0.90$. From the residual image (shown in lower panel of Fig. 5) we can see that in general, the residuals decrease, the hints of the ring remain and the ansae are better defined. The bump remains unfitted with the functions included in the model, which is expected given that it is caused by a ring and the bar ansae. The parameters derived from every model analysed are shown in Table 1.

4.1 NIR colour gradient

Fig. 9 shows the $J - K_s$ colour profile of the host galaxy of FBQS J164442.5+261913. The AGN contribution has been subtracted using the best-fitting model for each band.

In general, as we move from the centre to the outer parts of the host galaxy, we can see that the colour decreases from $J - K_s = 4.33$ down to 3.45 mag at $R = 1.20$ arcsec, showing that the central region (bulge) is the reddest of the host galaxy. From $R = 1.20$ arcsec towards larger radii, the colour increases up to a local maximum of $J - K_s = 3.63$ mag at $R = 1.55$ arcsec. We link this increase in colour to the bar, since here is where it has its maximum influence

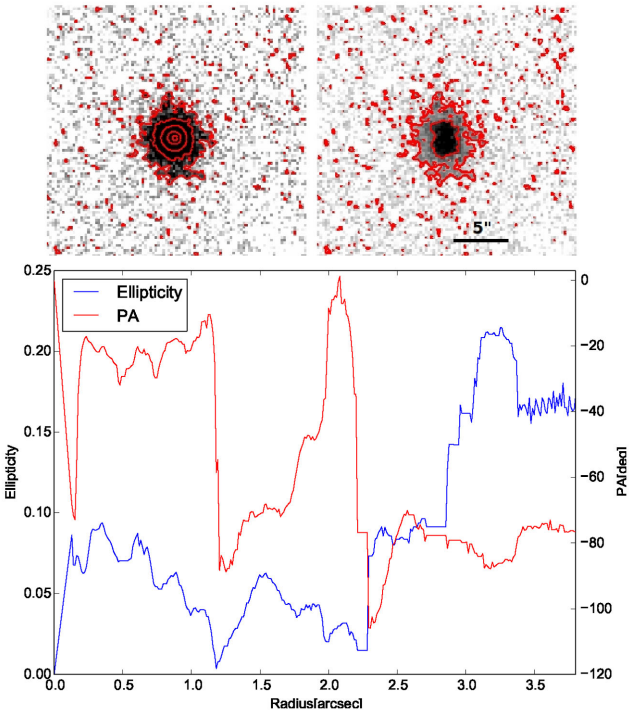

Figure 7. In top panels, we compare the observed K_s-band image (top left), with an image in K_s-band where the AGN and bulge models have been subtracted (top right). The bar becomes visible on the underlying disc if the AGN and bulge contributions are subtracted. In the lower panel, we show the average profiles of ellipticity ϵ (blue line) and PA (red line) obtained with ELLIPSE from K_s band plotted against the isophote major axis.

(see Fig. 8). A second increase in colour is observed in the bar region from $R = 2.20$ to 2.85 arcsec, with a maximum of $J - K_s = 3.80$ mag. Between 2.85 arcsec $< R <$ 3.15 arcsec, a blue region is observed that corresponds to eastern feature (inside the ring) in Figs 4 and 5. We observe a last local minimum at $R = 3.30$ arcsec with a colour $J - K_s = 3.80$ mag. We associate this colour to the ring, with no influence of the ansae since, according to observations by Martinez-Valpuesta et al. (2007), ansae do not show any colour enhancement (probably because they are a dynamical phenomena). Finally, as we move outward, the disc becomes bluer, reaching an average colour $J - K_s = 3.70$ mag.

5 THE HOST GALAXY OF FBQS J164442.5+261913

According to the results shown in Table 1, the host of FBQS J164442.5+261913 can be classified as a barred lenticular galaxy (SB0). In addition to the ansae morphology, that is frequent in S0 galaxies (∼40 per cent of S0) as found by Laurikainen et al. (2007), both the bulge and the disc fulfil the characteristics for lenticular galaxies presented in Laurikainen et al. (2010). They also find that, as in spirals (Hunt, Pierini & Giovanardi 2004; Noordermeer & van der Hulst 2007), the luminosity of the bulge in S0s correlate to the luminosity of their discs. According to such correlation ($M_{K,disc} = 0.63 M_{K,\mathrm{bulge}} + 9.3$), the bulge of FBQS J164442.5+261913 should have a disc with an absolute magnitude $M_{K,\,disc} = -24.55 \pm 0.20$, consistent with the absolute magnitude derived through the morphological analysis in this work ($M_{K,\,disc} = -24.85 \pm 0.25$).

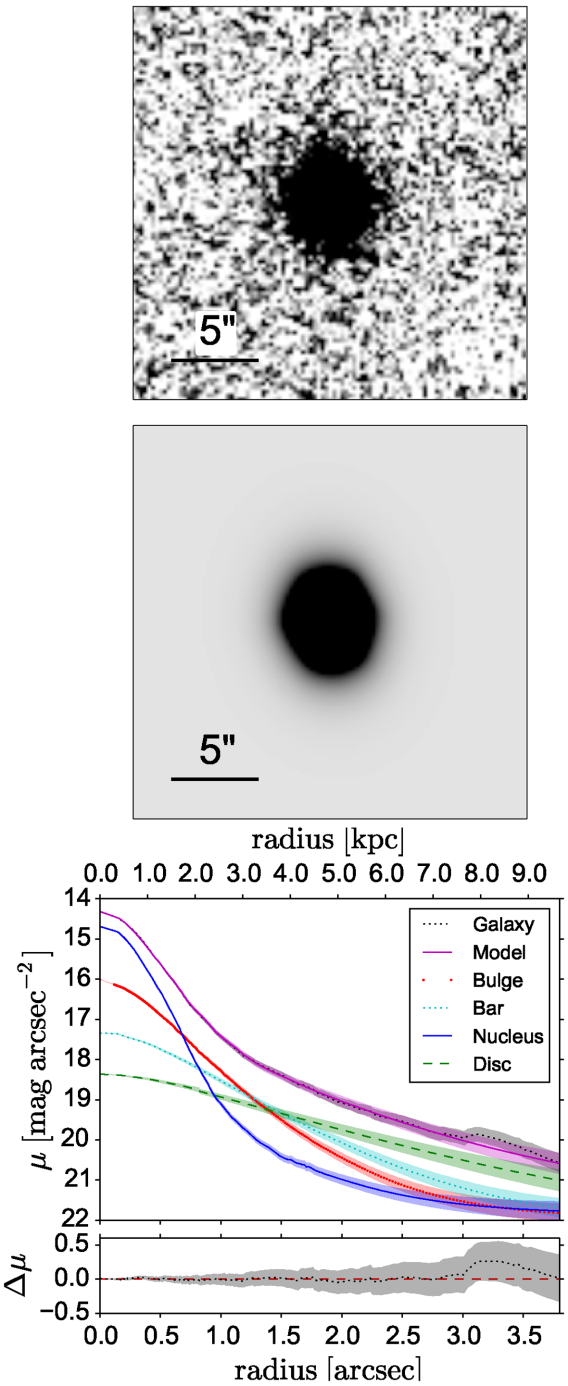

Figure 8. Model 4 (AGN+bulge+disc+bar) for the K_s band. Top panel shows the observed image. Middle panel shows our model image. Lower row shows the azimuthally averaged surface brightness profiles of the target, the model and the subcomponents of the model (top panel) and its residuals (bottom panel). Symbols are explained in the plots.

The parameters derived in this work for the components of FBQS J164442.5+261913 are consistent with those of pseudo-bulges. Weinzirl et al. (2009) find a connection with pseudo-bulges and small Sérsic indices ($n < 2.0$), consistent with $n = 1.8 \pm 0.31$ for J band and $n = 1.9 \pm 0.35$ for K_s band, derived for FBQS J164442.5+261913. Independently, Fisher & Drory (2008) find that pseudo-bulges and their discs are associated through their effective radius and scalelengths as $r_{\mathrm{eff}}/h_r = 0.21 \pm 0.10$ consistent

Table 1. Best-fitting parameters for model 1 (PSF only), model 2 (PSF + bulge), model 3 (PSF + bulge + disc) and model 4 (PSF + bulge + disc + bar). Parameter errors appear in parentheses[a].

Parameter	Model 1		Model 2		Model 3		Model 4[b]
	J	K_s	J	K_s	J	K_s	K_s
$m_{\rm AGN}$	15.65	14.28	16.67	14.39	16.67	14.80	14.38
	(0.33)	(0.34)	(0.38)	(0.41)	(0.43)	(0.38)	(0.24)
$m_{\rm bulge}$	–	–	15.70	13.86	17.77	14.55	14.97
	–	–	(0.37)	(0.39)	(0.40)	(0.39)	(0.32)
$m_{\rm disc}$	–	–	–	–	16.28	14.33	14.90
	–	–	–	–	(0.35)	(0.38)	(0.25)
$m_{\rm bar}$	–	–	–	–	–	–	15.32
	–	–	–	–	–	–	(0.42)
$R_{\rm eff}$ [arcsec kpc^{-1}]	–	–	0.95/2.40	0.82/2.07	0.38/0.96	0.30/0.76	0.43/1.10
	–	–	(0.23/0.58)	(0.27/0.68)	(0.13/0.32)	(0.14/0.35)	(0.14/0.34)
h_r [arcsec kpc^{-1}]	–	–	–	–	2.62/6.65	3.04/7.68	3.19/8.10
	–	–	–	–	(0.45/1.14)	(0.40/1.01)	(0.47/1.20)
$n_{\rm bulge}$	–	–	2.58	2.71	1.80	1.95	1.90
	–	–	(0.40)	(0.42)	(0.31)	(0.38)	(0.35)
$n_{\rm bar}$	–	–	–	–	–	–	1.17
	–	–	–	–	–	–	(0.30)
$\epsilon_{\rm bar}$	–	–	–	–	–	–	0.59
	–	–	–	–	–	–	(0.06)
χ^2_ν	4.250	3.927	1.785	1.645	1.160	1.300	1.181
	(0.032)	(0.033)	(0.030)	(0.031)	(0.027)	(0.029)	(0.022)

Notes. [a]Parameter errors are estimated following procedure from Section 3.1.1.
[b]Model 4 is only shown for K_s band, since no stellar bar is detected in J band.

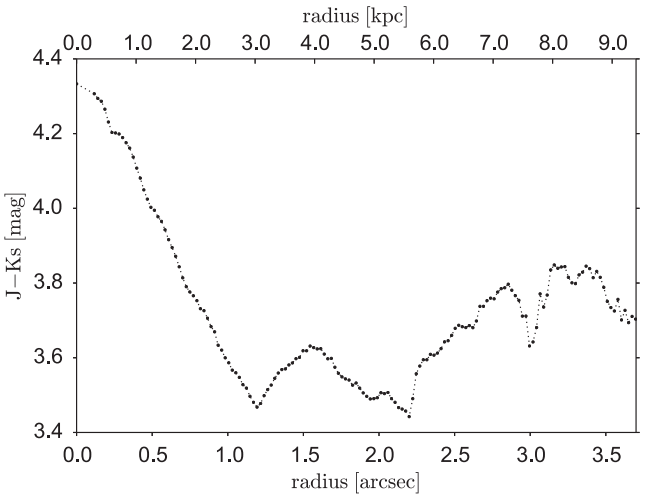

Figure 9. The radial $J - Ks$ colour profile of the host galaxy of FBQS J164442.5+261913. The AGN contribution has been subtracted from the best-fitting model of each band.

with FBQS J164442.5+261913 ($r_{\rm eff}/h_r = 0.14 \pm 0.07$ for J band and $r_{\rm eff}/h_r = 0.14 \pm 0.06$ for K_s band). On the contrary, they found that classical bulges have large $r_{\rm eff}/h_r$ ratios ($r_{\rm eff}/h_r = 0.45 \pm 0.28$). Additionally, when we compare the structural parameters of Table 1, with the results in La Barbera et al. (2010), we find that FBQS J164442.5+261913 lies below the Kormendy relation (either for J as for K_s band), consistent with Gadotti (2009) who find that pseudo-bulges do not tend to follow the Kormendy relation. Finally, if a galaxy hosts a pseudo-bulge, its centre should be mostly Population I material (young stars, gas and dust; Kormendy & Ho 2013). If we bear in mind that, in cases of high recent starburst, supergiants contribute to K-band luminosity (Minniti & Rix 1996), then the $J - K_s$ colour gradient of the host galaxy of FBQS J164442.5+261913, is in agreement with the latter pseudo-bulge classification criteria, where we see that, in the central region, K_s-band luminosity is stronger in comparison to J band than in any other region of the galaxy.

So far, only one galaxy, able to launch a relativistic jet powerful enough to accelerate particles up to γ-ray energies, is known to host a pseudo-bulge: PKS 2004−447 (Kotilainen et al. 2016). Nevertheless, León Tavares et al. (2014) do not discard that the γ-NLSy1 1H 0323+342 is also hosted by a pseudo-bulge.

We now evaluate whether the parameters derived for the bar in FBQS J164442.5+261913 are in accordance with those for active early-type galaxies. Using the maximum ellipticity of the ellipse fits to the bar region as bar length (Marinova & Jogee 2007), we find that the length of the bar in FBQS J164442.5+261913 is $r_{\rm bar} = 8.13 \pm 0.25$ kpc, if we normalized it to the disc scalelength h_r, we obtain $r_{\rm bar}/h_r = 1.00 \pm 0.06$. On the other hand, we can calculate the bar strength $f_{\rm bar}$ (Abraham & Merrifield 2000, see also Whyte et al. 2002; Laurikainen et al. 2007; Aguerri, Méndez-Abreu & Corsini 2009; Hoyle et al. 2011) defined as

$$f_{\rm bar} = \frac{2}{\pi}\{\arctan[(b/a)^{-0.5}] - \arctan[(b/a)^{0.5}]\}, \quad (3)$$

where b/a is the minor to major axis ratio of the bar. We obtain a bar strength $f_{\rm bar} = 0.17 \pm 0.03$. According to e.g. Aguerri et al. (2009) and Laurikainen et al. (2007), the bar in FBQS J164442.5+261913 is long and weak, consistent with S0 galaxies as found by Laurikainen, Salo & Rautiainen (2002).

The bar in FBQS J164442.5+261913 might be related to the ring through resonances (Athanassoula et al. 2010, and references therein), given that secular evolution is likely the main evolutionary process that is currently in progress in its host galaxy. Therefore, the ring-like feature might be the result of gas redistribution by angular momentum transport driven by the bar (i.e. a ring constructed by a rotating bar interacting with the disc gas). In this scenario, the gas

is moved by the bar into orbits near dynamical resonances (for a review, see Athanassoula, Machado & Rodionov 2013).

The main resonances are the Inner Lindblad Resonance (ILR) $\Omega_{\rm ILR} = \Omega_{\rm bar} - \kappa/2$, the Outer Lindblad Resonance (OLR) $\Omega_{\rm OLR} = \Omega_{\rm bar} + \kappa/2$ (Buta & Combes 1996) and the Ultra Harmonic Resonance (UHR) $\Omega_{\rm UHR} = \Omega_{\rm bar} - \kappa/4$, where $\Omega_{\rm bar}$ is the bar pattern speed and κ is the epicyclic frequency (Lindblad 1974). The latter is located close to corotation (Sellwood 2013), i.e. where the disc and the bar corotate.

Observations state that bars end near corotation (Kent 1987; Merrifield & Kuijken 1995; Sempere, Combes & Casoli 1995; Gerssen, Kuijken & Merrifield 1999; Debattista & Williams 2004; Gerssen 2002; Corsini, Debattista & Aguerri 2003), and can drive structures such as inner rings approximately at the UHR (Kormendy & Kennicutt 2004). Therefore, the feature located at $R = 3.20$ arcsec, might be consistent with that of an inner ring.

Another scenario for the ring formation in FBQS J164442.5+261913 is a minor merger event. Athanassoula, Puerari & Bosma (1997) show that the interaction of a small satellite galaxy on a barred galaxy can produce a ring that encloses the bar. Also, Mapelli, Rampazzo & Marino (2015) show that minor mergers with gas-rich satellites might explain the formation of rings in lenticular galaxies. This scenario is supported by the residuals in J-band (see Fig. 4), where a feature of surface brightness $\mu = 21.0 \pm 0.5$ mag arcsec^{-2} is shown about ∼5.15 arcsec/13.10 kpc east from the centre of FBQS J164442.5+261913 (resembling the Seyfert galaxy NGC 1097 whose light distribution is strongly affected by a small satellite galaxy; Higdon & Wallin 2003). This feature seems to interrupt the shape of the ring in the eastern part of the galaxy and even cause the colour enhancement at 3.0 arcsec.

An alternative and more likely scenario was proposed by Marino et al. (2011) for their sample of lenticular galaxies. The formation of the ring might be a joint effect of secular evolution driven by the bar and gas accreted from a small satellite galaxy (or many). Moreover, since S0 galaxies lack of an own gas reservoir (unlike spirals), this scenario also explains the origin of the gas needed to grow a massive bulge ($M_J = -22.42 \pm 0.40$ and $M_{Ks} = -24.21 \pm 0.32$) and activate the black hole in FBQS J164442.5+261913, as well as the way this gas is channelled to the most central parts of the galaxy (i.e. through angular momentum transport driven by the bar; Shlosman, Begelman & Frank 1990; Ohta et al. 2007).

We finally observe that the parameters of the bar and the ring hosted by FBQS J164442.5+261913, are similar to the bar of PKS 2004−447 (Kotilainen et al. 2016) and the ring in 1H 0323+342 (León Tavares et al. 2014). While the bars of PKS 2004−447 and FBQS J164442.5+261913, are $r_{\rm bar} \approx 7.80$ kpc and $r_{\rm bar} = 8.13 \pm 0.25$ kpc (taking the length of the bar as the maximum in the ellipticity profile), respectively, with absolute K_s-band magnitude of $K_{\rm bar} = -23.44 \pm 0.38$ and -23.86 ± 0.52, respectively; the rings of 1H 0323+342 and FBQS J164442.5+261913, are ∼8.24 and ∼8.13 kpc, respectively. Moreover, PKS 2004−447 shows an arm-like feature, whose origin might be related to a minor merger event (see fig. 19 of Athanassoula et al. 1997) and that, at some point, might become a ring, similar to the feature shown in FBQS J164442.5+261913.

According to the most accepted processes for jet formation, the Blandford–Znajek (BZ; Blandford & Znajek 1977; MacDonald & Thorne 1982; Penna, Narayan & Sądowski 2013) and the Blandford–Payne (BP; Blandford & Payne 1982) mechanisms, the jet launching and collimation requires very massive black holes with high spins and strong magnetic fields. All of this require major mergers to occur, which fits well with previous observations (McLure et al. 2004; Sikora et al. 2007) and the jet formation paradigm (where powerful relativistic jets are launched from giant elliptical galaxies; Marscher 2009). However, it comes completely at odds with the morphology of FBQS J164442.5+261913, with a bar and a disc, that lacks of a classical bulge and with a black hole mass (as estimated by the FWHM of its BLR lines and the continuum luminosity; Yuan et al. 2008) $M_{\rm BH} \sim 8 \times 10^6\,{\rm M}_\odot$ (although, previous studies show that values $M_{\rm BH} \gtrsim 10^8\,{\rm M}_\odot$ could be obtained when estimating its black hole mass by different methods; Baldi et al. 2016; Calderone et al. 2013).

6 SUMMARY

We have performed a detailed photometric analysis of the γ-NLSy1 FBQS J164442.5+261913. We use deep NIR imagery in J and K_s bands taken with the NIR camera NOTcam on the NOT. The main results of this analysis are as follows.

(i) The surface brightness distribution of FBQS J164442.5+261913 is best fitted by a model resulting from a sum of a nuclear source, a bulge and a disc. Additionally to these components, a stellar bar in the K_s-band image is detected and modelled. The morphological parameters derived from our analysis show that the bulge, the disc and the bar of the host galaxy of FBQS J164442.5+261913 fulfil the characteristics of SB0 galaxies.

(ii) We find that the Sérsic index and the relations between bulge and disc for FBQS J164442.5+261913 are in good agreement with those of pseudo-bulges. Therefore, the bulge in the host galaxy of FBQS J164442.5+261913 is statistically most likely to be pseudo.

(iii) In both J and K_s bands, we detect a ring enclosing the bar that is interrupted by, what it seems to be, a recent minor merger that might hint to the formation process of such inner ring, as suggested by Athanassoula et al. (1997).

(iv) When comparing the ring and bar in FBQS J164442.5+261913 to the ring and bar in 1H 0323+342 and PKS 2004−447 (the only two γ-NLSy1 whose morphology have been analysed until now), we find similarities regarding size and magnitude. Likewise, PKS 2004−447 shows an arm-like feature, whose origin might be related to a minor merger event and that, at some point, might become a ring, similar to the inner ring in FBQS J164442.5+261913.

We conclude that the prominent bar in the host galaxy of FBQS J164442.5+261913 has mostly contributed to its overall morphology driving a strong secular evolution, which plays a crucial role in the onset of the nuclear activity and the growth of its massive (pseudo) bulge. Minor mergers, in conjunction, are likely to provide the necessary fresh supply of gas to the central regions of the host galaxy.

Although our findings strongly suggest that secular evolution is the main process taking place in FBQS J164442.5+261913, our available data are insufficient to address some other questions as whether its (pseudo) bulge shows an increased star formation activity or if it is rotation-dominated (as it should, given its disky origin; Kormendy & Ho 2013). Therefore, we encourage different wavelengths imaging and integral field spectroscopy observations to this galaxy and the whole sample of radio-loud NLSy1s.

ACKNOWLEDGEMENTS

We thank Kari Nilsson who provided expertise that assisted this work. We acknowledge support by CONACyT research grant 151494 (Mexico), CONACyT program for PhD studies and Finnish

Centre for Astronomy with ESO (FINCA). This research is based on observations made with the Nordic Optical Telescope, operated by the Nordic Optical Telescope Scientific Association at the Observatorio del Roque de los Muchachos, La Palma, Spain, of the Instituto de Astrofísica de Canarias. This publication makes use of data products from the Two Micron All Sky Survey.

REFERENCES

Abdo A. A. et al., 2009, ApJ, 707, L142
Abraham R. G., Merrifield M. R., 2000, AJ, 120, 2835
Aguerri J. A. L., Méndez-Abreu J., Corsini E. M., 2009, A&A, 495, 491
Antón S., Browne I. W. A., Marchã M. J., 2008, A&A, 490, 583
Athanassoula E., Puerari I., Bosma A., 1997, MNRAS, 286, 284
Athanassoula E., Romero-Gómez M., Bosma A., Masdemont J. J., 2010, MNRAS, 407, 1433
Athanassoula E., Machado R. E. G., Rodionov S. A., 2013, MNRAS, 429, 1949
Bade N., Fink H. H., Engels D., Voges W., Hagen H.-J., Wisotzki L., Reimers D., 1995, A&AS, 110, 469
Baldi R. D., Capetti A., Robinson A., Laor A., Behar E., 2016, MNRAS, 458, L69
Barazza F. D., Jogee S., Marinova I., 2008, ApJ, 675, 1194
Bertin E., Arnouts S., 1996, A&AS, 117, 393
Blandford R. D., Payne D. G., 1982, MNRAS, 199, 883
Blandford R. D., Znajek R. L., 1977, MNRAS, 179, 433
Bruce V. A. et al., 2012, MNRAS, 427, 1666
Buta R., Combes F., 1996, Fundam. Cosm. Phys., 17, 95
Calderone G., Ghisellini G., Colpi M., Dotti M., 2013, MNRAS, 431, 210
Corsini E. M., Debattista V. P., Aguerri J. A. L., 2003, ApJ, 599, L29
Crenshaw D. M., Kraemer S. B., Gabel J. R., 2003, AJ, 126, 1690
Debattista V. P., Williams T. B., 2004, ApJ, 605, 714
Elmegreen B. G., Elmegreen D. M., Hirst A. C., 2004, ApJ, 612, 191
Fisher D. B., Drory N., 2008, in Funes J. G., Corsini E. M., eds, ASP Conf. Ser. Vol. 396, Formation and Evolution of Galaxy Disks. Astron. Soc. Pac., San Francisco, p. 309
Gadotti D. A., 2009, MNRAS, 393, 1531
Gerssen J., 2002, in Athanassoula E., Bosma A., Mujica R., eds, ASP Conf. Ser. Vol. 275, Disks of Galaxies: Kinematics, Dynamics and Peturbations. Astron. Soc. Pac., San Francisco, p. 197
Gerssen J., Kuijken K., Merrifield M. R., 1999, MNRAS, 306, 926
Graham A. W., Driver S. P., 2005, PASP, 22, 118
Greene J. E., Ho L. C., Barth A. J., 2008, ApJ, 688, 159
Häussler B. et al., 2007, ApJS, 172, 615
Higdon J. L., Wallin J. F., 2003, ApJ, 585, 281
Hoyle B. et al., 2011, MNRAS, 415, 3627
Hunt L. K., Pierini D., Giovanardi C., 2004, A&A, 414, 905
Jogee S., Kenney J. D. P., Smith B. J., 1999, ApJ, 526, 665
Kaspi S., Smith P. S., Netzer H., Maoz D., Jannuzi B. T., Giveon U., 2000, ApJ, 533, 631
Kent S. M., 1987, AJ, 93, 1062
Knapen J. H., Shlosman I., Peletier R. F., 2000, ApJ, 529, 93
Kormendy J., Ho L. C., 2013, ARA&A, 51, 511
Kormendy J., Kennicutt R. C. Jr., 2004, ARA&A, 42, 603
Kotilainen J. K., Hyvönen T., Falomo R., Treves A., Uslenghi M., 2011, A&A, 534, L2
Kotilainen J. K., León-Tavares J., Olguin-Iglesias A., Baes M., Anorve C., Chavushyan V., Carrasco L., 2016, ApJ, 832, 157
La Barbera F., de Carvalho R. R., de La Rosa I. G., Lopes P. A. A., 2010, MNRAS, 408, 1335
Laine S., Shlosman I., Knapen J. H., Peletier R. F., 2002, ApJ, 567, 97
Laor A., 2000, ApJ, 543, L111
Laurikainen E., Salo H., Rautiainen P., 2002, MNRAS, 331, 880
Laurikainen E., Salo H., Buta R., Knapen J. H., 2007, MNRAS, 381, 401
Laurikainen E., Salo H., Buta R., Knapen J. H., Comerón S., 2010, MNRAS, 405, 1089
León Tavares J. et al., 2014, ApJ, 795, 58
Lindblad P. O., 1974, in Shakeshaft J. R., ed., Proc. IAU Symp. 58, The Formation and Dynamics of Galaxies. Reidel, Dordrecht, p. 399
McLure R. J., Willott C. J., Jarvis M. J., Rawlings S., Hill G. J., Mitchell E., Dunlop J. S., Wold M., 2004, MNRAS, 351, 347
MacDonald D., Thorne K. S., 1982, MNRAS, 198, 345
Mapelli M., Rampazzo R., Marino A., 2015, A&A, 575, A16
Marino A., Bianchi L., Rampazzo R., Thilker D., Annibali F., Bressan A., Buson L. M., 2011, Ap&SS, 335, 243
Marinova I., Jogee S., 2007, ApJ, 659, 1176
Marscher A. P., 2009, in Belloni T., ed., Lecture Notes in Physics, Vol. 794, The Jet Paradigm. Springer-Verlag, Berlin, p. 173
Martinez-Valpuesta I., Knapen J. H., Buta R., 2007, AJ, 134, 1863
Mathur S., Fields D., Peterson B. M., Grupe D., 2012, ApJ, 754, 146
Mattox J. R. et al., 1996, ApJ, 461, 396
Menéndez-Delmestre K., Sheth K., Schinnerer E., Jarrett T. H., Scoville N. Z., 2007, ApJ, 657, 790
Merrifield M. R., Kuijken K., 1995, MNRAS, 274, 933
Minniti D., Rix H. W., 1996, Proceedings of the ESO/MPA Workshop, Spiral Galaxies in the Near-IR. Springer-Verlag, Berlin
Noordermeer E., van der Hulst J. M., 2007, MNRAS, 376, 1480
Ohta K., Aoki K., Kawaguchi T., Kiuchi G., 2007, ApJS, 169, 1
Olguín-Iglesias A. et al., 2016, MNRAS, 460, 3202
Orban de Xivry G., Davies R., Schartmann M., Komossa S., Marconi A., Hicks E., Engel H., Tacconi L., 2011, MNRAS, 417, 2721
Osterbrock D. E., Pogge R. W., 1985, ApJ, 297, 166
Peng C. Y., Ho L. C., Impey C. D., Rix H.-W., 2011, Astrophysics Source Code Library, record ascl:1104.010
Penna R. F., Narayan R., Sądowski A., 2013, MNRAS, 436, 3741
Pogge R. W., 2000, New Astron. Rev., 44, 381
Rix H.-W., Rieke M. J., 1993, ApJ, 418, 123
Sellwood J. A., 2013, Planets, Stars and Stellar Systems, Vol. 5: Galactic Structure and Stellar Populations, p. 923
Sempere M. J., Combes F., Casoli F., 1995, A&A, 299, 371
Sheth K., Regan M. W., Scoville N. Z., Strubbe L. E., 2003, ApJ, 592, L13
Shlosman I., Begelman M. C., Frank J., 1990, Nature, 345, 679
Sikora M., Stawarz Ł., Lasota J.-P., 2007, ApJ, 658, 815
Skrutskie M. F. et al., 2006, AJ, 131, 1163
Weinzirl T., Jogee S., Khochfar S., Burkert A., Kormendy J., 2009, ApJ, 696, 411
Whyte L. F., Abraham R. G., Merrifield M. R., Eskridge P. B., Frogel J. A., Pogge R. W., 2002, MNRAS, 336, 1281
Wozniak H., Friedli D., Martinet L., Martin P., Bratschi P., 1995, A&AS, 111, 115
Yuan W., Zhou H. Y., Komossa S., Dong X. B., Wang T. G., Lu H. L., Bai J. M., 2008, ApJ, 685, 801

This paper has been typeset from a TEX/LATEX file prepared by the author.